# Buildup of incoherent dissipative solitons in ultrafast fiber lasers

Zhiqiang Wang,[1,*] K. Nithyanandan,[2] Aurélien Coillet,[1] Patrice Tchofo-Dinda,[1] and Philippe Grelu[1,†]
[1]*Laboratoire Interdisciplinaire Carnot de Bourgogne, UMR 6303 CNRS, Université Bourgogne Franche-Comté, 9 Avenue Alain Savary, F-21078 Dijon, France*
[2]*LIPhy–Laboratoire Interdisciplinaire de Physique, UMR 5588 CNRS, Université Grenoble Alpes, F-38400 Saint Martin d'Hères, France*

(Received 12 July 2019; published 30 January 2020)

The self-formation of incoherent laser pulses appears paradoxical, involving both a strong instability and a temporal localization process. Incoherent pulse regimes are nevertheless recurrent within ultrafast fiber laser dynamics. In this paper, we bring decisive experimental data, by recording in real time the buildup dynamics of incoherent pulses under different cavity dispersion regimes. Our measurements highlight different dominant mechanisms at play. Whereas soliton pulse shaping contributes to creating a chaotic bunch of pulses in the anomalous dispersion regime, incoherent pulses in the normal dispersion regime follow strongly turbulent dissipative dynamics. Numerical simulations reproduce qualitatively well the final buildup stage of observed dynamics. By displaying common dynamical features as well as disparities, these results support the development of a general concept of incoherent dissipative solitons.

DOI: 10.1103/PhysRevResearch.2.013101

## I. INTRODUCTION

Ultrafast fiber lasers are being primarily developed as compact, efficient, stable mode-locked optical sources that are useful for countless applications ranging from medicine, telecom, and spectroscopy to material processing and range finding [1]. In parallel, during the past 15 years or so, the fiber laser platform has led to the discovery of a wide range of intriguing pulsed regimes lying in the territory between the conventional mode-locked and non-mode-locked regimes, driving a considerable interest in the fundamental areas of ultrafast laser physics and nonlinear dynamics [2].

In the conventional mode-locked laser operation, the cavity contains a single traveling pulse, which retakes the same profile evolution along successive cavity round trips. Such stability can be understood with the notion of a dissipative soliton, a general concept that finds a vast number of applications in nonlinear photonics and beyond [3]. The dissipative soliton usually manifests as a stable focus attracting state, providing long term stability and robustness to the traveling pulse. The flexible balance design of a dissipative soliton allows stable mode locking in counterintuitive parameter ranges, such as in the normal dispersion regime, leading to record high-energy pulse generation in fiber oscillators [4].

Nevertheless, as the domain of cavity parameters is explored, numerous bifurcations of the dissipative soliton dynamics can take place. Some bifurcations are abrupt, such as the multiple pulsing transitions that lead to an augmented number of traveling pulses per round trip, typically when the pump power is increased [5,6]. Other bifurcations are smoother, such as the onset of long-period oscillations, following, for instance, a Hopf bifurcation that transforms a stable focus into a limit-cycle attractor [7]. Combining the two sorts of bifurcations still represents a possibility, as attested to by the recent investigations of oscillating and vibrating *soliton molecules* in ultrafast lasers [8–10].

Abrupt bifurcations can also lead to chaotic-pulse dynamics. In some situations, a strong competition between instability and localizing physical effects takes place to maintain, on average, a localized short or ultrashort pulse in its moving reference frame. Illustrations of chaotic-pulse dynamics include the so-called soliton explosions [11,12], dissipative rogue waves [13–15], and noiselike pulse (NLP) emission [16–23]. Observed within a wide range of laser cavity architectures, these chaotic-pulse laser regimes can be linked to the existence of universal strange attractors [24]. As a matter of fact, despite the persistence of a defined round trip time for the traveling pulse, these laser regimes can no longer be qualified as mode locked. Therefore, it is instructive to compare them based on the loss of coherence. A laser operating in the soliton explosion regime can still be qualified as partially mode locked, since between explosive events, successive output pulses remain relatively close. Discovered in 1997 [16], the NLP emission in lasers is characterized by a complete loss of mutual coherence between successive pulses [17]. This intriguing regime displays the extreme competition between a strong instability and temporal localization, yet it is generally self-starting and quasistationary in the long run. Considered initially as a scientific curiosity, NLP emission subsequently attracted considerable attention, with attempts to identify its fundamental origin as well as to exploit its potentialities of high-energy and wideband short-pulse generation from a compact fiber laser system [18–23].

*wangzhiqiang@njupt.edu.cn
†philippe.grelu@u-bourgogne.fr

*Published by the American Physical Society under the terms of the Creative Commons Attribution 4.0 International license. Further distribution of this work must maintain attribution to the author(s) and the published article's title, journal citation, and DOI.*

The physical origins of NLP seem multifarious, reflecting the diversity of laser cavity architectures and parameters where such incoherent laser pulse regimes have been found. Consequently, there should be marked differences among dynamics sharing such denomination. Until recently, these differences were largely hidden behind the curtain of averaged spectral measurements and limited temporal resolution, which provided only incomplete experimental information about the internal dynamics of ultrashort pulses. The late spread of accessible real-time ultrafast measurements, such as the time-stretch dispersive Fourier transform (DFT) [25] and time-lens techniques [26], has entailed a major surge of investigations on ultrafast cavity dynamics, including the buildup of mode-locked pulses and soliton molecules [27–31]. Recent studies have also shown a close connection between NLP and the generation of optical rogue waves, indicating a strong overlap between the different chaotic-pulse dynamics, rather than well-defined frontiers [32–35]. In that respect, the denomination of *incoherent dissipative solitons* has recently been proposed to encompass them [23].

In this article, we bring decisive experimental data by recording the buildup dynamics of NLPs under different cavity dispersion regimes. Displaying common dynamical features as well as disparities, these data support the broad concept of incoherent dissipative solitons. The latter represents a general category of localized, quasistationary yet chaotic structures. In the framework of the present study, we show that the denomination of noiselike pulses already covers various types of dynamics, according to the dispersion regime. This is done through the comparison of the buildup and quasistationary dynamics in both normal and anomalous dispersion regimes, also supported by numerical simulations. Such diversity pleads toward the introduction of a more general concept, involving a chaotic attractor, which provides stability over the long-timescale observation, but maintains strong chaos at short evolution times.

Our measurements employ the time-stretch DFT optical characterization technique and highlight important differences with buildup transitions previously observed in the case of mode locking [27–31]. We highlight the major impact of the chromatic dispersion sign: Whereas soliton pulse shaping contributes to forming a chaotic-pulse bunch in the anomalous dispersion regime, incoherent pulses in the normal dispersion regime follow turbulent dynamics involving strongly dissipative effects. Numerical simulations reproduce qualitatively well the observed dynamics, from the final buildup stage to the quasistationary chaotic regime.

## II. EXPERIMENTS

### A. Experimental setup

The setup, sketched in Fig. 1, consists of an erbium-doped fiber ring laser, which operates in the 1.53–1.58-$\mu$m wavelength range, and its ultrafast-characterization instrumentation. To emit short pulses, the laser cavity includes a mechanism of ultrafast saturable absorption, based here on the nonlinear polarization evolution (NPE) that takes place in the optical fibers [36]. Followed by polarization discrimination, NPE produces an effective ultrafast saturable absorber effect.

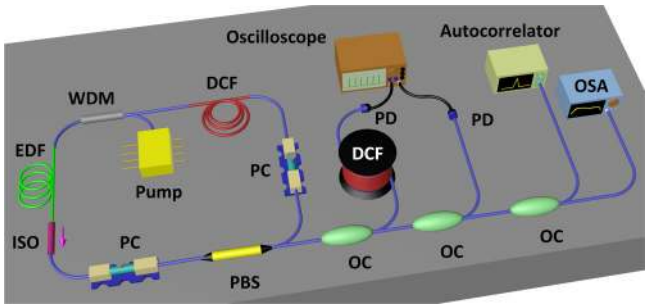


FIG. 1. Schematic of the ultrafast fiber laser experiment. EDF: erbium-doped fiber; DCF: dispersion-compensation fiber; ISO: polarization-independent isolator; PC: all-fiber polarization controller; PBS: polarization beam splitter; OC: optical coupler; PD: fast photodiode; OSA: optical spectrum analyzer.

The laser gain is provided by a 2-m-long erbium-doped fiber (EDF, normal dispersion $D = -12.5\,\mathrm{ps\,nm^{-1}\,km^{-1}}$) pumped with a 600-mW 980-nm diode laser. A polarization-insensitive isolator ensures unidirectional laser propagation, whereas the setting of polarization controllers (PCs) tunes the nonlinear transfer function of the effective saturable absorber, allowing one to access a wide range of ultrafast laser dynamics. A segment of dispersion-compensating fiber (DCF, $D = -108\,\mathrm{ps\,nm^{-1}\,km^{-1}}$) adjusts the total cavity dispersion. In the following, its length is 2.42 (0.88) m for the normal (anomalous) average dispersion regime, yielding a net cavity dispersion $\beta_2 = 0.115(-0.33)\ \mathrm{ps}^2$ at the 1550-nm wavelength, and a fundamental repetition rate frequency of 13.44 (15.58) MHz, corresponding to a round trip time of 74.39 (64.15) ns, respectively. The other fibers are standard single-mode fibers (SMF, anomalous dispersion $D = 17\,\mathrm{ps\,nm^{-1}\,km^{-1}}$). In each round trip time window, the output laser pulse is stretched by propagating through a 6345-m-long DCF that provides a total dispersion of $769\,\mathrm{ps}^2$. Thus, in the dispersive far-field limit, the spectral profile becomes mapped into the time domain and is detected with a high-speed 45-GHz photodiode (PD) plugged into a 6-GHz 40-GSa/s (giga-samples per second) real-time oscilloscope. The scale of wavelength-to-time mapping is 1.46 nm/ns, yielding an electronic-based spectral resolution of 0.3 nm. The output laser pulses are also detected directly with a 12.5 GHz PD and visualized on the oscilloscope.

The cavity architecture, a dispersion-managed fiber ring laser using nonlinear polarization evolution, can be considered as a standard configuration. Such cavity can operate in the fundamental mode-locking regime, as well as in the multiple pulse operation: the operation regime depends strongly on the polarization controller setting as well as on the pumping power level, besides a major influence of the path-averaged chromatic dispersion. It is also known that the laser cavity dynamics can bifurcate toward chaotic-pulse regimes under large pumping power, i.e., pumping power well beyond the single-pulse mode-locking threshold [18,19,32]. In the following, we focus on the intriguing incoherent pulse formation that reveals itself from such standard ultrafast fiber laser architecture. At large pumping power, it turns out that the incoherent noiselike pulse generation becomes the most represented pulse regime from our laser setup; i.e., it exists for a large range of

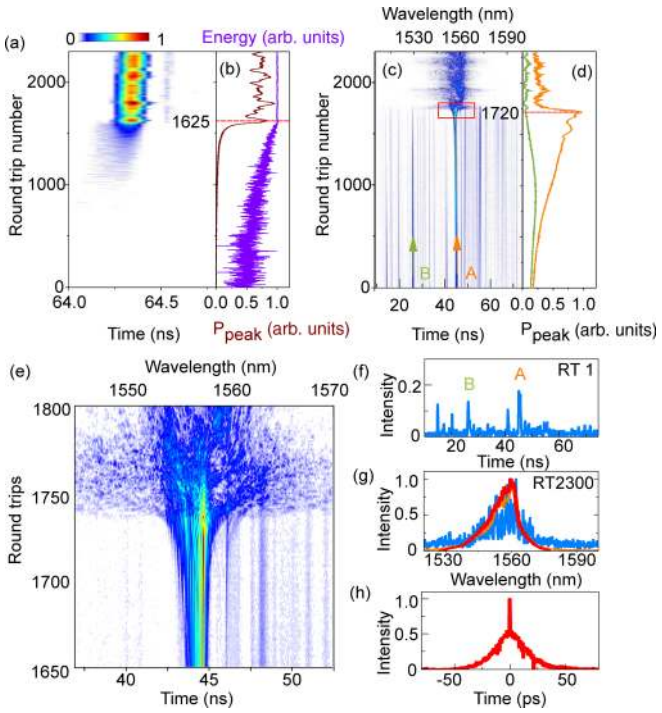


FIG. 2. Buildup dynamics of an incoherent short pulse in the normal dispersion cavity regime. Temporal evolution of (a) optical pulse intensity (in color scale); (b) normalized intracavity energy (violet line) and pulse peak intensity (brown line); (c) DFT output (optical intensity, in color scale) zoomed in (e). (d) Evolution of the peak intensity for the dominant pulse (A, amber) and for a competing pulse precursor (B, green). (f) Optical intensity distribution at the first round trip (RT 1); (g) single-shot spectrum at RT 2300 (blue curve), compared with the average of 500 consecutive single-shot spectra (orange) and the OSA-recorded spectrum (red); (h) multishot optical autocorrelation.

polarization controller settings, in contrast to mode-locked states that require a precise setting of the polarization controllers.

### B. Incoherent pulse buildup in the normal dispersion regime

Let us begin with the normal dispersion regime case, where the domain of existence of incoherent pulses is the most extended with respect to the settings of intracavity PC. The incoherent pulsed laser operation is self-starting for pump powers above 150 mW. Several characteristic stages of the pulse buildup process can be identified. This is illustrated by Fig. 2, which displays the buildup of an incoherent ∼20-ps-long short pulse after the electric intensity driving the pump diode has been switched on from 0 to 225 mW.

The first transient stage is dominated by *pulse amplification and competition*, from round trip (RT) 1 to RT ∼ 1625 on Figs. 2(a)–2(d), and is similar to the initial stage occurring in the standard mode-locking transition [27]. We notice many long-lived pulses of various amplitudes on the background, as also shown on Fig. 2(f). Note that the first round trip displayed does not coincide in time with the pump switch-on. Instead, the initiation of trace recording by the oscilloscope is determined by a triggering level that probes the imminence of the pulse buildup. Therefore, the oscilloscope is set up to record starting 120 $\mu$s before the trigger. This means that the oscilloscope keeps in memory ∼1620 traces before the triggering time, in order to capture the pulse precursor amplification and competition stage. During this stage, the total cavity energy increases, with large but decreasing fluctuations, until it reaches a nearly constant value at RT ∼ 1625. One of the pulses precursors, denoted as pulse A, wins the gain competition, while other background pulses such as pulse B are first amplified, then gradually annihilated after RT ∼ 1000. The pulse precursors, whose typical duration is in the nanosecond range, carry a narrow sub-nm spectral width, so that the 6.3-km-long DCF does not provide a far-field dispersive regime to them.

The following stage is characterized by *spectral broadening processes*. It can be decomposed in two phases: an exponential spectral broadening phase, and an explosive spectral broadening phase that is first revealed here. First, from RT ∼ 1625 to RT ∼ 1720, while the pulse energy saturates the gain, the pulse peak intensity exhibits large fluctuations, as seen in Fig. 2(b). Simultaneously, the optical spectrum broadens, as shown in the DFT recording of Fig. 2(e). These features result from complex nonlinear pulse dynamics involving pulse breakups and collisions, which are faintly reflected by the recorded fluctuations of the optical intensity (limited by the 66-ps rise time of the oscilloscope), but will be evidenced in the simulations presented hereafter. The DFT peak power in Fig. 2(d) increases up to a maximum at RT ∼ 1720, then depletes. This depletion coincides with the rapid spectral broadening, clearly visible in Fig. 2(e). The DFT output gradually shifts into the far-field regime, displaying relevant optical spectral information at the end of this substage. This first phase of spectral broadening evolution is similar to that observed in conventional mode locking [27,30,37]. However, the second spectral broadening phase is specific and sets up the chaotic-pulse regime. From RT ∼ 1720 onward, the optical spectrum profile becomes highly irregular, then literally explodes within a few round trip times, gaining an order of magnitude in spectral width as well as displaying a chaotic evolution from one round trip to the next, which appears from RT ∼ 1730 in Fig. 2(e). Interestingly, these two spectral broadening phases do overlap, with a core spectral content that continues to broaden, then disseminates, from RT ∼ 1730 to RT ∼ 1780.

Compared with the buildup of mode-locked pulses [27,30,37], we do not observe frequency beating dynamics, due in our case to the incoherence of the pulse during the final buildup stage. In addition, we note that the vanishing of residual nanosecond pulses takes ∼50 RT, significantly longer than in the mode-locking transition. After the second phase of spectral broadening, from RT ∼ 1780, the NLP propagation regime is established in a quasistationary way, which means that successive averaged measurements will yield the same information, namely, the average optical spectrum [see the matching red and amber curves in Fig. 2(g)] and the average optical autocorrelation, in Fig. 2(h). Nevertheless, the variability of successive single-shot spectra reflects the strongly chaotic dynamics and the incoherent nature of the short pulse. Complementarily, the average autocorrelation trace in Fig. 2(h) shows that the intrapulse coherence time of ∼500 fs

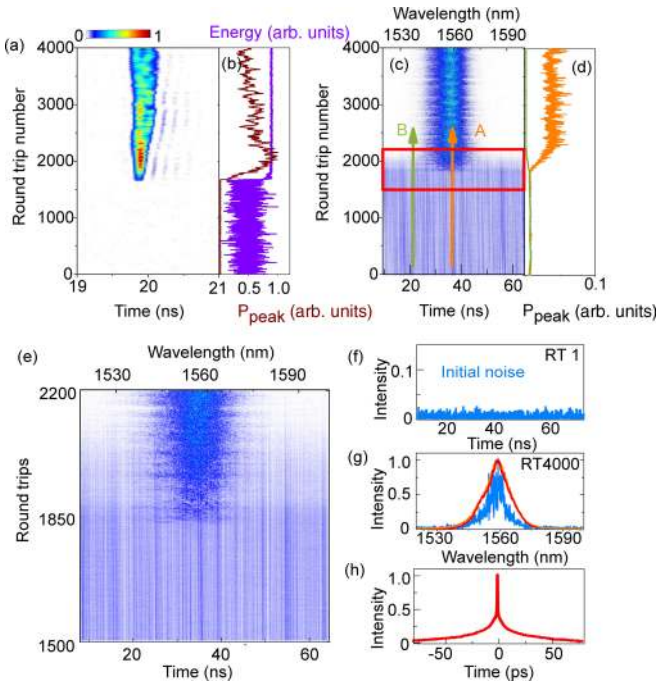


FIG. 3. Buildup dynamics of an incoherent short pulse in the anomalous dispersion cavity regime. Evolution of (a) pulse intensity; (b) intracavity energy (violet) and pulse peak intensity (brown); (c) DFT output (in color scale). (d) Evolution of the peak intensity, for pulse precursors A and B; (e) magnification of the DFT trace; (f) initial intensity distribution; (g) single-shot spectrum at RT 4000 (blue curve) and the averaging of 500 consecutive spectra (orange) compared with the averaged spectrum recorded by the OSA (red); (h) averaged optical autocorrelation.

(central sharp peak) is much shorter than the pulse average temporal extension of 22 ps.

### C. Incoherent pulse buildup with anomalous dispersion

In the normal dispersion cavity regime, pulse shaping results from an intricate balance among gain, loss, dispersion, and nonlinearity. In contrast, simpler pulse shaping can take place in the anomalous dispersion regime, largely influenced by the interplay between the chromatic dispersion and the Kerr nonlinearity. Therefore, we expect the buildup of incoherent pulses in an anomalous cavity to be qualitatively different. Using the same recording procedure, now for an anomalous cavity dispersion $\beta_2 = -0.33\,\mathrm{ps}^2$ and a maximum pump power of 200 mW, we obtain the buildup evolution displayed in Fig. 3.

The stage of *pulse amplification* displays a more abrupt transition than in the previous case. The cavity initially features a highly fluctuating background, rather than well-identified pulse precursors. Over a relatively long lapse of time, here from RT 1 to RT $\sim$ 1675, the amplification and competition processes seem ineffective, as seen, for instance, in the evolution of the energy for competing fluctuations A and B of Fig. 3(d). Suddenly, within a few cavity round trips, pulse A emerges from the time domain, as seen in Fig. 3(a), clamping the total cavity energy [violet curve in Fig. 3(b)]. The subsequent *spectral broadening* stage takes about the next $\sim$200 round trips. In contrast to the normal dispersion case, spectral broadening and chaotic evolution take place simultaneously, also accompanied by a very gradual disappearance of the noisy background and competing precursor pulses; see Fig. 3(e). Therefore, the present transition appears completely different from the mode-locking transitions [27–31].

As can be anticipated from a transition relying on stochastic processes, the buildup time as well as the details of the dynamics varies from one experimental recording to another. However, the various dynamical phases follow the universal trends described, with the chromatic dispersion being the most crucial parameter of which significant changes are observed.

## III. NUMERICAL SIMULATIONS

To gain more insight into the formative stage of the incoherent pulse buildup, we perform numerical simulations using a lumped scalar laser model [8,10]. Propagation in the fibers are modeled by an extended nonlinear Schrödinger equation:

$$\frac{\partial \psi}{\partial z} = -\frac{i}{2}\beta_2 \frac{\partial^2 \psi}{\partial t^2} + i\gamma|\psi|^2\psi + \frac{g(z)}{2}\psi, \qquad (1)$$

where $\psi$ is the slowly varying electric field, $z$ the propagation distance, and $t$ the time in the pulse group velocity reference frame. $\gamma$ and $\beta_2$ are the Kerr nonlinearity and dispersion coefficients, respectively. We used measured dispersion values for $\beta_2$, and calculated nonlinear coefficients $\gamma = 3.6\times10^{-3}\,\mathrm{W}^{-1}\,\mathrm{m}^{-1}$ and $1.3\times10^{-3}\,\mathrm{W}^{-1}\,\mathrm{m}^{-1}$ for EDF and SMF, respectively. The gain $g(z)$ includes saturation, spectral

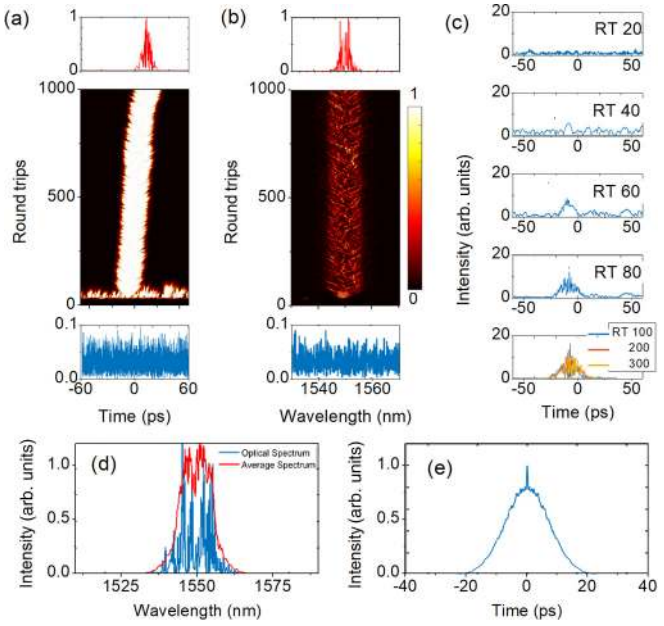


FIG. 4. Simulation results of incoherent pulse buildup in the normal dispersion cavity regime, with $P_i = 45$ mW and $P_{sat} = 10$ W. (a) Temporal (see also video in Supplemental Material [38]) and (b) spectral evolution from the initial noise that is displayed on the bottom row. Top row: quasistationary chaotic regime. (c) Temporal intensity profile at some characteristic round trip times (RT). (d) Optical spectrum and (e) autocorrelation trace averaged over the 500 last cavity round trips.

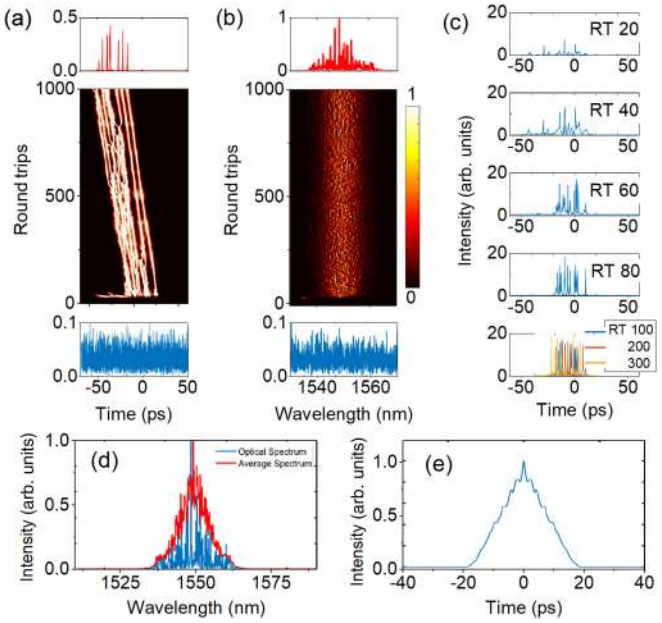


FIG. 5. Simulation results of incoherent pulse buildup in anomalous dispersion laser cavity at $P_{in} = 55\,\mathrm{mW}$ and $P_{\mathrm{sat}} = 10\,\mathrm{W}$. (a) Temporal (see also video file in Supplemental Material [38]) and (b) spectral evolution from noise displayed in the bottom rows. The top rows display the field characteristics at round trip 1000. (c) Temporal evolution at some characteristic round trip times (RT). (d) Optical spectrum and (e) autocorrelation trace averaged over the 500 last cavity round trips.

filtering, and longitudinal dependence. The saturable absorber is modeled by the following instantaneous transfer function: $T = P_0\ /P_i = T_0 + \Delta T \times P_i\ /(P_i + P_{\mathrm{sat}})$, with $P_i$ ($P_0$) being the instantaneous input (output) optical power, normalized as $P(z,t) = |\psi(z,t)|^2$. As typical values, we take $T_0 = 0.70$ for the low-intensity transmission and $\Delta T = 0.30$ as the absorption contrast. By assuming noise as the initial condition for the simulations, we tweak the lasing states by tuning the intracavity power $P_i$ and saturation power $P_{\mathrm{sat}}$.

The simulation results of the buildup of incoherent pulses in the normal dispersion regime are shown in Fig. 4. The amplification of noise leads to the emergence of numerous chaotic pulses that compete for the gain within the simulation temporal window. One pulse wins the competition and is further amplified, its peak power allowing to initiate the spectral broadening stage, which takes here about 50 RTs. Finally, we reach the quasistationary chaotic-pulse evolution, characterized by the average optical spectrum of Fig. 4(d) (red line) and optical autocorrelation of Fig. 4(e). To gain a complementary appreciation of the simulated buildup of the optical intensity in the time domain, see the movie in the Supplemental Material [38].

In the anomalous dispersion case (Fig. 5) we note that the transition from the noisy background to the incoherent picosecond pulse is more abrupt than in the normal dispersion case, which is consistent with the experimental recordings. Even more interesting, the transition reveals the shaping of numerous solitonlike pulses at an early stage, which combine to form the overall quasistationary incoherent pulse. This is markedly different from the incoherent pulse profile in the normal dispersion case, as the incoherent pulse is here a compact bunch of solitonlike pulses that collide, exchange energy, and move chaotically; see also the movie showing the evolution of the optical field intensity (Supplemental Material [38]).

The above numerical model is a standard propagation model for ultrashort pulses, which does not include the slow gain relaxation dynamics. In such model, one uses a sliding temporal window that represents only a small fraction of the whole cavity round trip time, i.e., around 100 ps, as compared with a cavity round trip over 60 ns. That window slides along the entire cavity at the pulse group velocity, meeting the various components described by their specific parameters, hence the denomination of a parameter-managed model. This procedure is not adapted to simulate the generation of long-lived pulse precursors, which are typically ∼100-ps- to ∼1-ns-long pulses and are distributed along the whole cavity, an initial stage also similar to that described in the case of conventional mode locking [26]. When major fluctuations reach the few-ps duration, both nonlinear and dispersive lengths come down to the order of a few cavity round trips. From there, the generic experimental traits of the spectral broadening and the chaotic evolution phases can be qualitatively well reproduced by the current model, namely:

(1) The abrupt transition from the pulse precursor (experiment) or from noise background (simulation) toward the pulse regime, which takes only a few tens of cavity round trips;

(2) the onset of a pulse instability, which unfolds during another few tens of cavity round trips, and leads to an incoherent pulse;

(3) the chaotic subsequent evolution that maintains a temporal localization, compatible with the notion of an incoherent dissipative soliton, which is characterized by average features (spectral and temporal extension) that can be defined typically for an averaging time on the order of 100 cavity round trips.

## IV. CONCLUSIONS

By resolving the buildup of incoherent laser pulses for two different cavity dispersion regimes, we have shown salient differences between the underlying pulse forming dynamics. Whereas major differences occur during the buildup stages, different spectrotemporal dynamics are also observed during the quasistationary chaotic regime. The two regimes imply different underlying mechanisms, which we describe in the light of the numerical simulations of the ultrafast cavity dynamics. The normal dispersion regime is characterized by the largest fluctuations, owing to the interplay of gain, self-phase modulation, and dispersion: smaller pulse constituents diffuse rapidly and vanish outside the main pulse extension, since being dispersed, their amplitude decreases and they get filtered out by the saturable absorber. In the anomalous dispersion regime, soliton pulse shaping is acting and maintains the integrity of pulses over much longer times. However, frequent pulse collisions entail highly varying amplitudes, which induces a pulse discrimination through the action of the nonlinear gain.

The existence of these very different physical mechanisms leading to quasistationary chaotic-pulse waveforms indicates that chaotic, NLPs exist in a much wider space of cavity

parameters than initially anticipated. Akin to the generalization of a variety of stable ultrashort laser dynamics into the broad concept of dissipative solitons, we find it useful to term noiselike pulses as incoherent dissipative solitons of ultrafast lasers. The incoherent dissipative soliton terminology indeed includes the notion of chaos—the noiselike evolution—as well as the notion of an attracting state that arises from the nonlinear gain and loss terms of a dissipative medium. The picture of a chaotic attractor helps to understand the transition from spectral broadening to chaotic evolution. The chaotic evolution, considered as a chaotic attractor, is therefore the destination of the transition. The chaotic attractor explains why the long-timescale observation will remain stable; i.e., successive multishot autocorrelations and optical spectra recordings (through a conventional optical spectrum analyzer) will yield nearly identical traces. The notion of a chaotic attractor explains also why successive laser switch-ons will yield the same long-timescale features, despite each buildup evolution being unique, and differs in the details with another one. From that onward, the incoherent dissipative soliton concept is ready to be applied to other nonlinear systems, involving other spatiotemporal dimensions. Like the dissipative soliton concept, the notion of an incoherent dissipative soliton is expected to stimulate research in multiple areas of nonlinear science and bring multiple analogies between them.

## ACKNOWLEDGMENTS

This work was supported by the Centre National de la Recherche Scientifique (CNRS), the Indo-French Centre for the Promotion of Advanced Research (IFCPAR/CEFIPRA Project No. 5104-2), the EIPHI Graduate School (ANR-17-EURE-0002), the Région Bourgogne, and the European Regional Development Fund (ERDF/FEDER).

[1] M. E. Ferman and I. Hartl, Ultrafast fiber lasers, Nat. Photon. **7**, 868 (2013).

[2] P. Grelu and N. Akhmediev, Dissipative solitons for mode-locked lasers, Nat. Photon. **6**, 84 (2012).

[3] *Dissipative Solitons, from Optics to Biology and Medicine*, edited by N. Akhmediev and A. Ankiewicz (Springer, Heidelberg, 2008).

[4] A. Chong, W. H. Renninger, and F. W. Wise, All-normal-dispersion femtosecond fiber laser with pulse energy above 20 nJ, Opt. Lett. **32**, 2408 (2007).

[5] A. Komarov, H. Leblond, and F. Sanchez, Multistability and hysteresis phenomena in passively mode-locked fiber lasers, Phys. Rev. A **71**, 053809 (2005).

[6] X. Liu, Hysteresis phenomena and multipulse formation of a dissipative system in a passively mode-locked fiber laser, Phys. Rev. A **81**, 023811 (2010).

[7] J. M. Soto-Crespo, M. Grapinet, Ph. Grelu, and N. Akhmediev, Bifurcations and multiple-period soliton pulsations in a passively mode-locked fiber laser, Phys. Rev. E **70**, 066612 (2004).

[8] K. Krupa, K. Nithyanandan, U. Andral, P. Tchofo-Dinda, and P. Grelu, Real-Time Observation of Internal Motion within Ultrafast Dissipative Optical Soliton Molecules, Phys. Rev. Lett. **118**, 243901 (2017).

[9] G. Herink, F. Kurtz, B. Jalali, D. R. Solli, and C. Ropers, Real-time spectral interferometry probes the internal dynamics of femtosecond soliton molecules, Science **356**, 50 (2017).

[10] Z. Q. Wang, K. Nithyanandan, A. Coillet, P. Tchofo-Dinda, and Ph. Grelu, Optical soliton molecular complexes in a passively mode-locked fibre laser, Nat. Commun. **10**, 830 (2019).

[11] S. T. Cundiff, J. M. Soto-Crespo, and N. Akhmediev, Experimental Evidence for Soliton Explosions, Phys. Rev. Lett. **88**, 073903 (2002).

[12] A. F. J. Runge, N. G. R. Broderick, and M. Erkintalo, Observation of soliton explosions in a passively mode-locked fiber laser, Optica **2**, 36 (2015).

[13] C. Lecaplain, Ph. Grelu, J. M. Soto-Crespo, and N. Akhmediev, Dissipative Rogue Waves Generated by Chaotic Pulse Bunching in a Mode-Locked Laser, Phys. Rev. Lett. **108**, 233901 (2012).

[14] A. Zavyalov, O. Egorov, R. Iliew, and F. Lederer, Rogue waves in mode-locked fiber lasers, Phys. Rev. A **85**, 013828 (2012).

[15] M. Liu, A. P. Luo, W. C. Xu, and Z. C. Luo, Dissipative rogue waves induced by soliton explosions in an ultrafast fiber laser, Opt. Lett. **41**, 3912 (2016).

[16] M. Horowitz, Y. Barad, and Y. Silberberg, Noiselike pulses with a broadband spectrum generated from an erbium-doped fiber laser, Opt. Lett. **22**, 799 (1997).

[17] A. Runge, C. Aguergaray, N. G. R. Broderick, and M. Erkintalo, Coherence and shot-to-shot spectral fluctuations in noise-like ultrafast fiber lasers, Opt. Lett. **38**, 4327 (2013).

[18] Y. Takushima, K. Yasunaka, Y. Ozeki, and K. Kikuchi, 87 nm bandwidth noise-like pulse generation from erbium-doped fiber laser, Electron. Lett. **41**, 399 (2005).

[19] L. M. Zhao, D. Y. Tang, T. H. Cheng, H. Y. Tam, and C. Lu, 120 nm bandwidth noise-like pulse generation in an erbium-doped fiber laser, Opt. Commun. **281**, 157 (2008).

[20] S. Kobtsev, S. Kukarin, S. Smirnov, S. Turitsyn, and A. Latkin, Generation of double-scale femto/pico-second optical lumps in mode-locked fiber lasers, Opt. Express **17**, 020707 (2009).

[21] T. North and M. Rochette, Raman-induced noiselike pulses in a highly nonlinear and dispersive all-fiber ring laser, Opt. Lett. **38**, 890 (2013).

[22] J. C. Hernandez-Garcia, O. Pottiez, and J. M. Estudillo-Ayalab, Supercontinuum generation in a standard fiber pumped by noise-like pulses from a figure-eight fiber laser, Laser Phys. **22**, 221 (2012).

[23] K. Krupa, K. Nithyanandan, and P. Grelu, Vector dynamics of incoherent dissipative optical solitons, Optica **4**, 1239 (2017).

[24] H. Wei, B. Li, W. Shi, X. Zhu, R. A. Norwood, N. Peyghambarian, and S. Jian, Hierarchy, dimension, attractor and self-organization—dynamics of mode-locked fiber lasers, arXiv:1606.00533.

[25] K. Goda and K. B. Jalali, Dispersive Fourier transformation for fast continuous single-shot measurements, Nat. Photon. **7**, 102 (2013).

[26] A. Tikan, S. Bielawski, C. Szwaj, S. Randoux, and P. Suret, Single-shot measurement of phase and amplitude by using a heterodyne time-lens system and ultrafast digital time-holography, Nat. Photon. **12**, 228 (2018).

[27] G. Herink, B. Jalali, C. Ropers, and D. R. Solli, Resolving the build-up of femtosecond mode-locking with single-shot spectroscopy at 90 MHz frame rate, Nat. Photon. **10**, 321 (2016).

[28] J. Peng and H. Zeng, Build-up of dissipative optical soliton molecules via diverse soliton interactions, Laser Photon. Rev. **12**, 1800009 (2018).

[29] P. Ryczkowski, M. Närhi, C. Billet, J.-M. Merolla, G. Genty, and J. M. Dudley, Real-time full-field characterization of transient dissipative soliton dynamics in a mode-locked laser, Nat. Photon. **12**, 221 (2018).

[30] J. Peng, M. Sorokina, S. Sugavanam, N. Tarasov, D. V. Churkin, S. K. Turitsyn, and H. Zeng, Real-time observation of dissipative soliton formation in nonlinear polarization rotation mode-locked fibre lasers, Commun. Phys. **1**, 20 (2018).

[31] X. Liu, X. Yao, and Y. Cui, Real-Time Observation of the Buildup of Soliton Molecules, Phys. Rev. Lett. **121**, 023905 (2018).

[32] C. Lecaplain and Ph. Grelu, Rogue waves among noiselike-pulse laser emission: An experimental investigation, Phys. Rev. A **90**, 013805 (2014).

[33] A. F. J. Runge, C. Aguergaray, N. G. R. Broderick, and M. Erkintalo, Raman rogue waves in a partially mode-locked fiber laser, Opt. Lett. **39**, 319 (2014).

[34] P. Wang, D. Hu, K. Zhao, L. Jiao, X. Xiao, and C. Yang, Dissipative rogue waves among noise-like pulses in a Tm fiber laser mode locked by a monolayer MoS2 saturable absorber, IEEE J. Sel. Top. Quantum Electron. **24**, 1800207 (2018).

[35] B. Li, J. Kang, S. Wang, Y. Yu, P. Feng, and K. K. Y. Wong, Unveiling femtosecond rogue-wave structures in noise-like pulses by a stable and synchronized time magnifier, Opt. Lett. **44**, 4351 (2019).

[36] P. D. Maker, R. W. Terhune, and C. M. Savage, Intensity-Dependent Changes in the Refractive Index of Liquids, Phys. Rev. Lett. **12**, 507 (1964).

[37] H. J. Chen, M. Liu, J. Yao, S. Hu, J. B. He, A. P. Luo, W. C. Xu, and Z. C. Luo, Buildup dynamics of dissipative soliton in an ultrafast fiber laser with net-normal dispersion, Opt. Express **26**, 2972 (2018).

[38] See Supplemental Material at http://link.aps.org/supplemental/10.1103/PhysRevResearch.2.013101 for the movie showing the simulated evolution of the optical field intensity over successive cavity round trips, in the normal and anomalous dispersion cases.